Open access • Journal Article • DOI:10.1007/BF02646396

Retained austenite and tempered martensite embrittlement — Source link

Gareth Thomas

Institutions: University of California, Berkeley

Published on: 01 Mar 1978 - Metallurgical and Materials Transactions A-physical Metallurgy and Materials Science (Springer-Verlag)

Topics: Bainite, Austenite, Martensite, Tempering and Quenching

Submitted to Metallurgical Transactions

LBL-5732
Preprint

RETAINED AUSTENITE AND TEMPERED MARTENSITE EMBRITTLEMENT

Gareth Thomas

October 1977

Prepared for the U. S. Department of Energy
under Contract W-7405-ENG-48

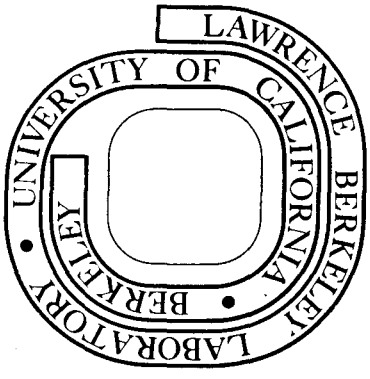

DISCLAIMER

RETAINED AUSTENITE AND TEMPERED MARTENSITE EMBRITTLEMENT

Gareth Thomas

Department of Materials Science and Mineral Engineering, College of Engineering, and Materials and Molecular Research Division, Lawrence Berkeley Laboratory, University of California, Berkeley, California

ABSTRACT

The problems of detecting the distribution of small amounts (5% or less) of retained austenite films around the martensite in quenched and tempered experimental medium carbon Fe/C/X steels are discussed and electron optical methods of analysis are emphasized. These retained austenite films if stable seem to be beneficial to fracture toughness. It has been found that thermal instability of retained austenite on tempering produces an embrittlement due to its decomposition to inter-lath films of M_3C carbides. The fractures are thus intergranular with respect to martensite but transgranular with respect to the prior austenite. The temperature at which this occurs depends upon alloy content. The effect is not found in Fe/Mo/C for which no retained austenite is detected after quenching, but is present in all other alloys investigated.

INTRODUCTION

In a systematic program of research using vacuum melted high purity Fe/C/X steels, the relation between microscopic features and tensile strength and fracture properties has been correlated, from which the substructure, whether dislocated or twinned, has been shown to be very important[1].

It is now well known that the presence of dislocated and twinned martensite substructures found in quenched steels depends upon composition, especially carbon[1-3] and the M_s-M_f temperature range. By proper design of these parameters the substructure and tensile properties can be controlled. In recent years it has also become apparent that small amounts of very finely dispersed films of retained austenite (γ) occupying about 0.01-0.05 volume fraction can be resolved at the interfaces between martensite laths in certain quenched and quenched and tempered experimental and commercial steels by sophisticated electron microscopic methods[4,5,6]. The result is somewhat surprising in cases where M_s temperature is quite high (>200°C) i.e., in steels containing mostly dislocated martensites. This observation of retained austenite, first reported for Fe/Cr/C experimental steels by McMahon and Thomas[4], has been linked to the fracture toughness properties for which at least empirically it is now known that stable retained austenite films can be beneficial[4,6,7]. McMahon and Thomas[4] also observed a loss in toughness upon tempering which they showed was correlated with the decomposition of the austenite with formation of interlath carbide films. This phenomenon has also been observed recently in 4340 and 300M steels[8] but was not found in Fe/Mo/C alloys[9].

It is the purpose of this paper to emphasize 1) that the detection and unique identification of these small amounts of interlath austenite is non-trivial and involves very careful electron microscopy and diffraction,

2) that such austenite films, if stable, can be beneficial to toughness and 3) that the thermal instability of interlath austenite, leading to carbides upon tempering, is a fairly general cause of tempered martensite embrittlement. This latter effect, to be detected, clearly depends on the ability to detect the original austenite.

IDENTIFICATION OF RETAINED AUSTENITE

When retained austenite is present in amounts greater than about 1-2%, it may be detected by classical x-ray methods[10], provided the grain size of the prior austenite is not too large (~0.1μm or more) or by refined magnetic measurements and other non-magnetic techniques, e.g., γ rays. Even if these methods detect austenite, they can not indicate any morphological characteristics. However, in cases where such methods fail to detect austenite, for example in medium or low carbon steels in which the microstructure consists of packets of dislocated martensite laths, careful electron microscopy and dark field analyses often show that these laths are separated by thin films of austenite[5].

It is important to emphasise, therefore, that such films of austenite may go undetected if x-rays and/or magnetic methods only are employed, or if only bright-field electron microscopy imaging* is carried out.

It has already been pointed out by Rao et al.[5] that careful selection of orientation and long exposure times are needed if austenite reflections are to be recorded and appropriate dark field imaging* done on austenite reflections. However, on-going research on a variety of steels (see Table I), has indicated that even greater care must be excercised because of the following:

1. In as-quenched and tempered martensitic steels the presence of carbides gives added reflections whose spacings coincide, or nearly

* In this paper the abbreviations BF and DF will be used for bright field and dark field imaging respectively.

so, with austenite. This will be especially true in dislocated martensites where M_s is usually >300°C when auto-tempering will occur upon quenching[1].

2. In many cases adjacent laths are twin related which not only causes extra martensite reflections to appear but also double diffraction spots which can add to the complexity of sorting out the structure.
3. The area contributing to the selected area diffraction pattern for a given beam diameter at the specimen is limited by spherical aberration and cannot be compensated for by using smaller selected apertures.

For conventional 100 kV TEM instruments, this is about 1-2μ but at high voltages it is considerably reduced due to the reduction in electron wavelength (e.g., ~0.2μ at 650 kV). Thus, the typical selected area diffraction (SAD) pattern of lath martensite obtained with a 100 kV microscope contains overlapping diffraction patterns from several crystals (laths) and often considerable arcing occurs in the pattern as a result of the internal strains and minor orientation differences of adjacent laths. All these factors contribute to the difficulty in identifying any austenite reflections. As shown earlier where multiple twinning in plate martensite was found[11] high voltage electron microscopy is of great advantage for identifying fine details, especially as martensite laths are frequently 0.5μ or less in width and so several laths normally contribute to 100 kV electron diffraction patterns [e.g. see fig. 1(b)].

As a result of these factors a typical 100 kv selected area diffraction (SAD) pattern can contain the following:

a) One or more martensite orientations including twin related ones.

b) doubly diffracted spots

c) faint austenite reflections

d) carbide reflections (e.g. 3 out of 6 possible variants of M_3C with $\{110\}\alpha$ habit or 3 out of 12 possible variants with $\{112\}\alpha$ habit)

e) multiple diffraction due to interactions from the above.

This latter problem (e) has already been emphasized for interpretation of phases in maraging steels by Cheng and Thomas[12]. As an illustration of these effects Fig. 1(a) shows a calculated composite pattern of retained austenite, cementite and martensite. The common orientation relationships which have been observed in the steels, are the Kurdjumov-Sachs for martensite-austenite and Bagaryatski for cementite-martensite and these have been utilized to plot Fig. 1(a). Fig. 1(b) shows an observed typical electron diffraction pattern at 100 kV obtained from an area containing only retained austenite and lath martensite. There are two lath martensite orientations contributing to the pattern, viz., $\langle 100\rangle\alpha$ and $\langle 111\rangle\alpha$ and the symmetrical $\{110\}\gamma$ is suitably indexed.

The problem to prove the existence of austenite by dark-field imaging is the choice of the correct reflection after identifying the pattern and distinguishing austenite reflections from all others. Obviously, the choice of an austenite reflection furthest removed from any others is needed especially in view of the problem of spherical aberration. From Fig. 1 it is clear that $(200)\gamma$ has a relatively large angular separation from other reflections and is the reflection to be utilized. This reflection is also far enough removed

from spots due to double diffraction which commonly occur close to the transmitted beam. It is necessary to use long exposure times taken at appropriate condenser lens defocussing settings for both the SAD pattern and dark-field (DF) image. Imaging exposures of 30 secs. or so are required. Figure 2 shows an example of such an analysis in which the $(200)\gamma$ dark field image clearly reveals the interlath austenite films which are more or less continuous throughout the packet[13]. Complete analysis of the microstructure in fact requires several DF images of the same area to be made in order to distinguish films of austenite, M_3C or interface double diffraction. For example, Fig. 3 shows an image where an interlath M_3C is found in an isothermally transformed steel[14]. It can be described morphologically as upper bainite. Comparing Fig. 3(b) with Fig. 2(b) it is clear that one can not deduce the presence of retained austenite just from the contrast and morphology alone but a detailed diffraction and dark-field analysis is required. Another example to emphasize this point is shown in Fig. 4, which shows that double diffraction gives interlath boundary contrast[13] which is not an intrinsic structural feature. Fig. 4(a) is the BF image of twin related laths in a packet martensite the two variants of which are revealed in figures 4(b) and (c). Fig. 4(d) is obtained from a doubly diffracted reflection whereby the interfaces between the two variants are imaged. The corresponding diffraction pattern Fig. 4(e) is analysed in Fig. 4(f). Figures 3,4 emphasise that dark-field imaging interpretation requires unique identification of the origin of the diffraction contributing

to that contrast. Thus, very careful transmission electron microscopic analysis is required in order to unambiguously identify the presence of thin films of retained austenite in steels when the volume fraction is of the order of 0.02-0.05.

RESULTS ON EXPERIMENTAL STEELS

1. Factors Affecting Retained Austenite and Its Significance on Toughness

The observations suggest that at least qualitatively the fracture toughness properties of martensite steels are improved due to the presence of stable interlath films of austenite. An important design parameter is therefore the control of such austenite as outlined in the following.

a. Effect of Composition:

It is well known that increasing the carbon content of steels above 0.5% increases the volume fraction of retained austenite following quenching to room temperature. The detrimental effects of retained austenite in high carbon steels wherein it transforms to plate (twinned) martensite under the influence of an applied load or isothermally are well recognized, (see e.g. ref. 15). However, in the experimental steels developed over the past 12 years (Table 1) wherein the composition of the steel is adjusted so as to produce dislocated martensite, such danger emanating from undesirable transformation products of unstable austenite is avoided. The retention of austenite in the as-quenched martensite can thus be beneficial.

An interesting example of the effect of composition on the amount of retained austenite and the consequent mechanical properties is obtained from the systematic study which has been

carried out of microstructure-mechanical property relationships of experimental Fe/C/X ternary alloys where X is a substitutional alloying element. These alloys are listed in Table 1. Fig. 5 shows that for a given strength level, the plane strain fracture toughness values of Fe/Cr/C steels are higher than those of Fe/Mo/C alloys. In both cases the martensite is dislocated. Careful electron metallography and diffraction had revealed[4,9] the existence of interlath films of austenite in the former whereas austenite could not be detected in the latter. The observed differences in the amounts of retained austenite in Fe/Cr/C steels vs. Fe/Mo/C steels can be partly reconciled with the fact that Cr is much less potent than Mo in limiting the austenite phase field[16]. Similarly, extensive amounts of interlath retained austenite has been detected in Fe/1Cr/1Mo/0.3C steels (Fig. 2) and again these steels showed[13] much superior Charpy impact energies compared to the Fe/Mo/C steels.

Mn and Ni are strong austenite stabilizers and are expected to promote retained austenite in the as-quenched structures if added to a steel. In the present studies on several specimens and several different regions within each specimen, retained austenite is observed to increase monotonically with Mn addition (up to 2%Mn studied) to the ternary Fe/4Cr/0.3C alloy. An example is shown in Fig. 6. A 5% Ni addition to this ternary alloy also increased the volume fraction of retained austenite about 10 times compared to the base alloy, as indicated in Fig. 6(e)*. Analysis of Figs. 1(b) and 7(f) shows that the Kurdjumov-Sachs orientation relationship between fcc austenite

* These results have been independently corroborated by the x-ray analyses of our alloys by Dr. R. L. Miller, (U.S. Steel). More details will be published later.

and martensite is obeyed. The significance of this increase in % austenite with respect to mechanical properties is illustrated in Fig. 7 which shows the increase in Charpy impact energy with Mn addition to the ternary alloy. Ternary alloys modified with Ni also showed improved impact toughness properties. Thus, the composition of the steel, in addition to influencing martensite substructure, plays a paramount role in controlling the amount of austenite in the alloy and consequently the mechanical properties.

b. Influence of Heat-Treatment and Grain-size:

Heat-treatment also plays a key role in determining the amount of retained austenite. Austenitizing temperatures high enough to dissolve all the carbides so keeping all the alloying elements in solution without undue grain growth are observed to increase the amount of retained austenite[4,6,17]. From a study of the effect of austenitizing treatment on the microstructure and properties of ternary Fe/Cr/C steels[17], it was concluded that retained austenite occurs in greater amounts in the high temperature (>1000°C) austenitised steels as compared to low temperature (~870°C) treated steels. These results are expected as a result of dissolution of M_7C_3 type carbides at higher temperatures. If the alloying elements are partly locked up in carbides and other precipitates, they will obviously have less effect on the amount of austenite following quenching. In the above steels the K_{IC} fracture toughness improved with austenitizing temperature until 1100°C although it could not be attributable singly or significantly to the increase in the amount of austenite.

Experimental double treatments which combine the benefits of

dissolving all the alloy carbides and a fine grain size showed the highest amounts of retained austenite[18, 13]. The stabilization of austenite by closely spaced boundaries in a fine grained steel are well documented in the literature[19]. Thus, if all carbides are in solution, a fine grained steel would be expected to contain more retained austenite compared to a coarse grained structure as is now observed.

It was also found that substantial amounts of retained austenite can be introduced in the microstructure by holding the steel in the martensite formation region (M_s-M_f) during quenching[20,21]. The combined effects of finer grain size and higher volume fraction of retained austenite yielded superior impact toughness and strength properties following grain refinement in Fe/1Cr/1Mo/0.3C steels[13].

2. Thermal Stability and Temper Martensite Embrittlement

In order to improve the toughness to strength ratio (which in turn increases the critical flaw size) steels are usually tempered following quenching although in many cases the experimental steels are designed for good fracture toughness properties in the as-quenched condition[1] (see Fig. 5). However, upon tempering most of these steels exhibit a temper martensite embrittlement around 350°C tempering [sometimes referred to as "the 500°F embrittlement" in commercial steels[22]]as summarised in Table 1. Such embrittlement is accompanied by a loss of toughness as shown in Fig. 8. Fig. 8(a) shows a minimum in Charpy impact energy in Fe/1Cr.1Mo/0.3C steel following 350°C tempering while Fig. 8(b) shows embrittlement at 300°C in the ternary

Fe/4Cr/0.3C steel and quaternary Fe/4Cr/0.3C + 0.5% alloys. This embrittlement is not the classic intergranular embrittlement due to impurity segregation and/or precipitation at the grain boundaries [22], i.e., the fractures are not necessarily intergranular, and occur even in the carefully vacuum melted experimental steels wherein the impurity content is much lower than most commercial steels. The embrittlement in these steels is transgranular and is attributed to the decomposition of retained austenite with the formation of interlath cementite (or M_3C) films as shown by the detailed electron microscopy analysis of Fig. 9. Such tempered structures are very much like those of upper bainite and are clearly undesirable (compare to Fig. 3). Typical fractographs are shown in Fig. 10 for Fe/Cr/C steels modified with Mn. Figs. 10(a) and (c) are the fractographs following 200°C tempering of 0.5%Mn and 2% Mn quaternary alloys while (b) and (d) are the fractographs, respectively, of the same alloys following 300°C tempering. At 200°C, the predominant fracture mode is dimpled rupture while at 300°C the fracture is mainly quasi-cleavage. The fracture behavior of these alloys correlates directly with the decomposition characteristics of austenite on tempering. At 300°C when most of the interlath austenite was found to be decomposed, the fractographs [Figs. 10(b) and (d)] can be interpreted in terms of fracture paths along the lath/packet boundaries as a consequence of the presence of carbide particles at these boundaries [23]. Thus the fracture path is intergranular with respect to martensite but of course transgranular with respect to prior austenite.

It appears that although grain refinement could decrease the severity of embrittlement[18], the thermal stability of the retained

austenite was unaffected and the actual occurrence of the toughness minima could not be alleviated even in fine grained alloys.

Thus, whatever the benefits of retained austenite are to toughness, these are lost if the austenite becomes unstable. Alloying additions which favor austenite stability should, therefore, improve fracture properties upon tempering. In the Fe/4Cr/0.3C alloy modified with quaternary additions of 5% Ni, retained austenite appears to be more stable and appreciable amounts of untransformed austenite are noticeable even up to 400°C. Consequently, the tempered martensite embrittlement in this case is very mild. Nickel is thus very beneficial in this regard (Table 1). At the present time the mechanism of the decomposition of austenite to form carbides is not known.

It was pointed out earlier that no retained austenite could be detected in the Fe/Mo/C alloys. Consistent with this observation, Fig. 11 shows that these alloys do not undergo tempered martensite embrittlement[24].

DISCUSSION

The austenite stability with respect to transformation to marensite on quenching must be related to two main factors:]) between M_s and M_f, the solute elements, especially carbon will segregate to the austenite lowering its M_s temperature, so driving M_f locally further and further down, eventually leading to regions of untransformed austenite remaining between martensite laths (chemical stabilization); b) accommodation of transformation strains by plastic deformation generating dislocations in austenite could also stabilize the austenite through mechanical stabilization[25,26]. Observations show that retained austenite is invariably heavily deformed [Figs. 6(a) through (e)].

On the other hand, the austenite stability with respect to decomposition into $\alpha + M_3C$ will decrease as the carbon content in austenite increases due to a higher chemical driving force for carbide nucleation. Likewise dislocations in austenite could assist heterogeneously in nucleation of carbides and the reaction $\gamma \rightarrow \alpha + M_3C$. The problem, therefore, is that the factors that minimize the $\gamma \rightarrow M_s$ transition will favor the $\gamma \rightarrow \alpha + M_3C$ transition. There is a serious lack of experimental evidence to document how the transformation of retained austenite is influenced by alloying--whether it transforms to fresh martensite, or bainitic ferrite + M_3C or normal ferrite + M_3C. It appears that alloying additions which discourage cementite nucleation and growth can postpone the on-set of tempered martensite embrittlement to a higher temperature. Examples of these elements from current research at Berkeley include Ni[18], Si and Al[27]. The carbon diffusivity in austenite and martensite as affected by the chemical affinity between carbon and other alloying elements is perhaps important. Mn increases the carbon diffusivity and promotes rapid nucleation and growth of cementite. Ni, Al and Si do otherwise by discouraging M_3C nucleation and growth to a higher temperature and thus, postpone the onset of tempered martensite embrittlement[18,27]. Further research along these lines will be fruitful in successfully exploiting the benefits of retained austenite on mechanical properties. In related research, retained austenite in steel has also been shown to be beneficial for stress corrosion cracking and it reduces the tendency for environment prone embrittlement[28,29].

SUMMARY AND CONCLUSIONS

1. Retained austenite exists in most as-quenched dislocated martensitic medium carbon alloy steels except Fe/Mo/C as stabilised fine inter-lath films. These films are usually detected only by detailed electron metallography.
2. These retained austenite films, provided they are stable, seem to be beneficial to fracture toughness.
3. Temper martensite embrittlement occurs when retained austenite decomposes at the lath boundaries to form M_3C. Alloying elements which disfavor M_3C precipitation and its growth appear to postpone the onset of the embrittlement to a higher tempering temperature. Thus, Mn,Cr promote its decomposition at a lower temperature while Si,Al and Ni postpone it to a higher temperature.
4. Those factors which promote austenite retention on quenching also favor its thermal instability on tempering.
5. These results on retained austenite indicate that the terminology, lath martensite, is probably incorrect and that each martensite crystal within a packet is independently nucleated. This aspect is discussed elsewhere[32].

ACKNOWLEDGEMENTS

I am especially grateful to the graduate students who have contributed so much to this alloy design program over the years. I particularly thank B. V. N. Rao for his assistance with this paper. The continued financial support of ERDA through the Lawrence Berkeley Laboratory and the steel companies who have produced the alloys to our specifications (Table 1) is gratefully acknowledged.

TABLE I

Range of Compositions (wt%) of Experimental Steels Studied in This Research

Carbon	Cr	Mo	Ni	Co	Mn	B	Temper Martensite Embrittlement Temp	Alloy † Source	Ref.
0.3	4	-	-	-	-	-	300°C	1,2*	18
0.3	4	-	-	-	0.5	-	300°C	2*	18
0.3	4	-	-	-	2.0	-	300°C	2*	18
0.3	4	-	5	-	-	-	400°C	2*	18
0.3	1	1	-	-	-	-	350°C	3*	13
0.3	1	1	-	-	-	.0016	350°C	3*	13
0.41	-	4.2	-	-	-	-	Not Observed	1*	24
0.43	-	2.2	-	-	-	-	Not Observed	1*	24
0.26	-	-	4.85	-	3.8	-	315°C	1	30
0.24	-	-	12.5	3.8	-	-	425°C	1*	31

† 1. Republic Steel Research Labs.

2. Daido Steel Company

3. Climax Molybdenum Company

* Vacuum melted.

REFERENCES

1. G. Thomas: Iron and Steel Intl., 1973, vol. 46, p. 451.

2. J. Nutting: J. of Iron and Steel Inst., 1969, vol. 207, p. 872.

3. G. Thomas: Met. Trans., 1971, vol. 2, p. 2373.

4. J. McMahon and G. Thomas: Proc. Intl. Conf. "The Microstructure and Design of Alloys", Cambridge, vol. 1, p. 180, Inst. of Metals, London, 1973.

5. B. V. Narasimha Rao, J. Y. Koo and G. Thomas: Proceedings Electron Microscopy Society of America, 33rd Annual Meeting, p. 30, Claitors Publishing Division, Baton Rouge, 1975.

6. G. Y. Lai, W. E. Wood, R. A. Clark, V. F. Zackay and E. R. Parker: Met. Trans., 1974, vol. 5, p. 1663.

7. D. Webster: Met. Trans., 1971, vol. 2, p 2097.

8. R. O. Ritchie and R. Horn: University of California, Berkeley, unpublished research, 1977.

9. R. A. Clark and G. Thomas: Met. Trans. A, 1975, vol. 6A, p. 969.

10. R. L. Miller: Trans. ASM, 1964, vol. 57, p. 892; ibid., 1968, vol. 61, p 592.

11. G. Thomas and S. K. Das, J. Iron and Steel Inst., 1971, vol. 209, p. 801.

12. L-Lin Cheng and G. Thomas: Trans ASM, 1968, vol. 61, p 14.

13. Y. L. Chen: Ph.D. Thesis, 1976, Univ. of California, Berkeley, LBL Report Number 5423.

14. R. W. Miller: M.S. Thesis, 1974, Univ. of California, Berkeley, LBL Report Number 3104.

15. G. Krauss and A. R. Marder: Met. Trans., 1971, vol. 2, p 2343.

16. E. C. Bain and H. W. Paxton: "Alloying Elements in Steel", 2nd Edition, American Soc. for Metals, Metals Park, 1966.

17. M. F. Carlson: M. S. Thesis (in progress), Univ. of California, Berkeley.

18. B. V. Narasimha Rao: Ph.D Thesis (in progress), Univ. of California, Berkeley.

19. W. C. Leslie and R. L. Miller: Trans. ASM, 1964, vol. 57, p. 972.

20. E. P. Klier and A. R. Troiano, Metals Technology, 1945, vol. 12, p 1.

21. B. V. Narasimha Rao, R. W. Miller and G. Thomas: Proc. of 16th Intl. Heat Treatment Conf. "Heat Treatment '76", The Metals Society (London), p 75.

22. J. R. Rellick and C. J. McMahon: Met. Trans., 1974, vol. 5, p 2439.

23. T. B. Cox and J. R. Low: Met. Trans., 1974, vol. 5, p 1457.

24. R. A. Clark, M. S. Thesis, 1973, Univ. of California, Berkeley, LBL Report Number 1801.

25. P. M. Kelly and J. Nutting: J. of Iron and Steel Inst., 1961, vol. 197, p 199.

26. B. Edmondson and T. Ko: Acta Met., 1954, vol. 2, p 235.

27. M. S. Bhat: Ph.D. Thesis, 1977, Univ. of California, Berkeley, LBL Report Number 6046.

28. D. Webster: AFC 77, 1969, Boeing Document D6-23973.

29. M. Castro: M. S. Thesis, 1977, Univ. of California, Berkeley, LBL Report Number 6012.

30. D. Huang and G. Thomas: Met. Trans., 1971, vol. 2, p 1587.

31. S. K. Das and G. Thomas: Trans. of ASM, 1969, vol. 62, p 659.

32. G. Thomas and B.V.N. Rao, International Conference on Martensitic Transformations Kiev, USSR, May, 1977, (in press), LBL-6242.

FIGURE CAPTIONS

Fig. 1(a) - Calculated electron diffraction pattern for martensite in $[\bar{1}11]$ orientation with retained austenite and widmanstatten cementite. (b) Indexed electron diffraction pattern of austenite (a) and martensite (m) reflections in Fe/1Cr/1Mo/0.3C steel quenched from 870°C into ice water (see Fig. 2).

Fig. 2 - Bright field image (a) and dark field image (b) of an Fe/1Cr/1Mo/0.3C steel quenched from 870°C into ice water. Note that the interlath retained austenite films do not show good contrast in the bright field image, but are very clear in the (200)γ dark-field image. The corresponding diffraction pattern is shown in Fig. 1(b).

Fig. 3 - Bainite in Fe/4Cr/0.4C steel isothermally transformed at 400°C, for 5 min. BF (a) and DF (b) images of a carbide reflection.

Fig. 4 - As-quenched martensite in Fe/1Cr/1Mo/0.3C alloy. (a) BF image of the twin related martensite laths, (b) DF image of one twin orientation using reflection A in (f), (c) DF image of the other twin orientation using reflection B in (f), and (d) DF image of a doubly diffracted beam C in (f). (f) is the analysis of SAD pattern in (e).

Fig. 5 - Relationship between plane strain fracture toughness and ultimate tensile strength. Note that the Fe/Cr/C alloy has superior properties to the Fe/Mo/C steel and to other commercially available high strength steels.

Fig. 6 - Variation of retained austenite in Fe/Cr/C ternary alloys modified with Mn and Ni (a) DF image of austenite in Fe/4Cr/0.3C (b) DF image of austenite in steel modified with 0.5%Mn (c) DF of austenite in steel modified with 1.0%Mn (d) DF image of austenite in steel modified with 2.0%Mn (e) DF image of austenite in steel modified with 5.0%Ni

(f) indexed SAD pattern with retained austenite reflections (a) of modified steel with 2% Mn.

Fig. 7 - Variation of Charpy impact energy with Mn addition to the ternary Fe/Cr/C steels. The data for 5%Ni addition is also included. All the steels are grain refined by double treatments.

Fig. 8 - Charpy impact energy variation with tempering in (a) Fe/1Cr/1Mo/0.3C steels (b) Fe/4Cr/0.3C and with 0.5%Mn alloys.

Fig. 9 - Example of the decomposition of retained austenite into blocky M_3C and ferrite, (a) BF (b) DF (c) SAD (d) analysis in Fe/Cr/C steels modified by Mn addition.

Fig. 10 - Fractographs of Fe/4Cr/0.3C + Mn alloys (a) and (b) are of 0.5Mn alloy at 200°C and 300°C tempering respectively and (c) and (d) are of 2%Mn alloy at 200°C and 300°C tempering respectively.

Fig. 11 - Charpy-V-Notch impact toughness as a function of tempering temperature in Fe/Mo/C alloys.

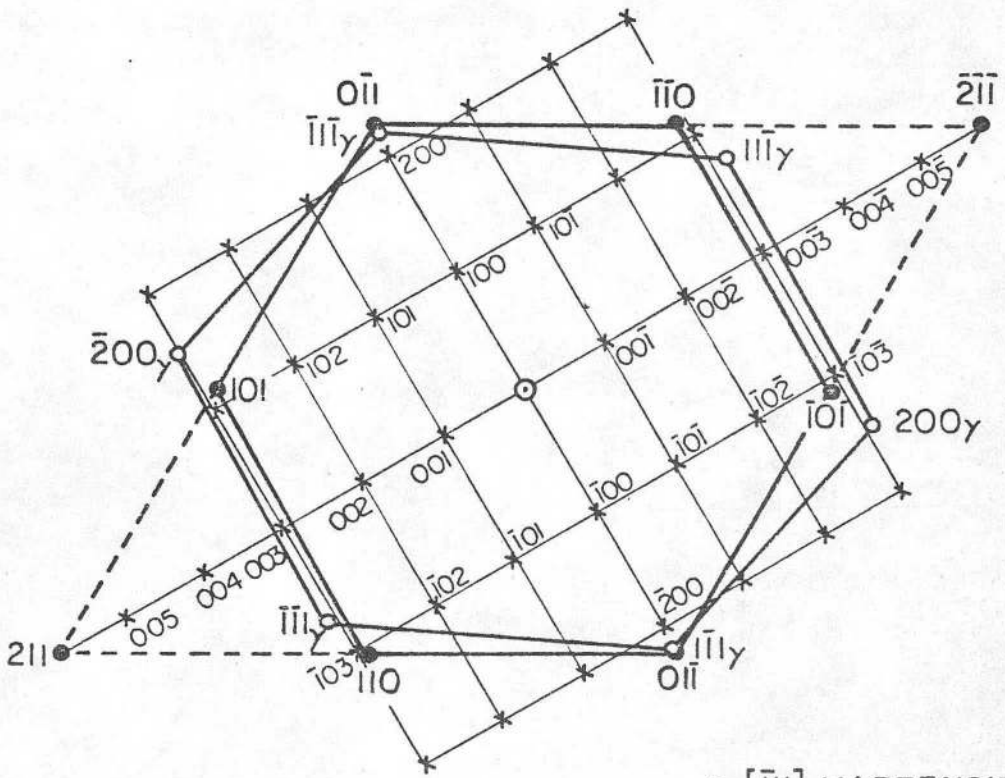

- [$\bar{1}$11] MARTENSITE
- o [011] AUSTENITE
- x [0$\bar{1}$0] CEMENTITE

$(01\bar{1})_\alpha \parallel (1\bar{1}1)_\gamma$

$(\bar{1}11)_\alpha \parallel (011)_\gamma$

$(0\bar{1}1)_\alpha \parallel (100)_c$

$(\bar{1}11)_\alpha \parallel (0\bar{1}0)_c$

$(211)_\alpha \parallel (001)_c$

XBL758-6830

Fig. 1(a)

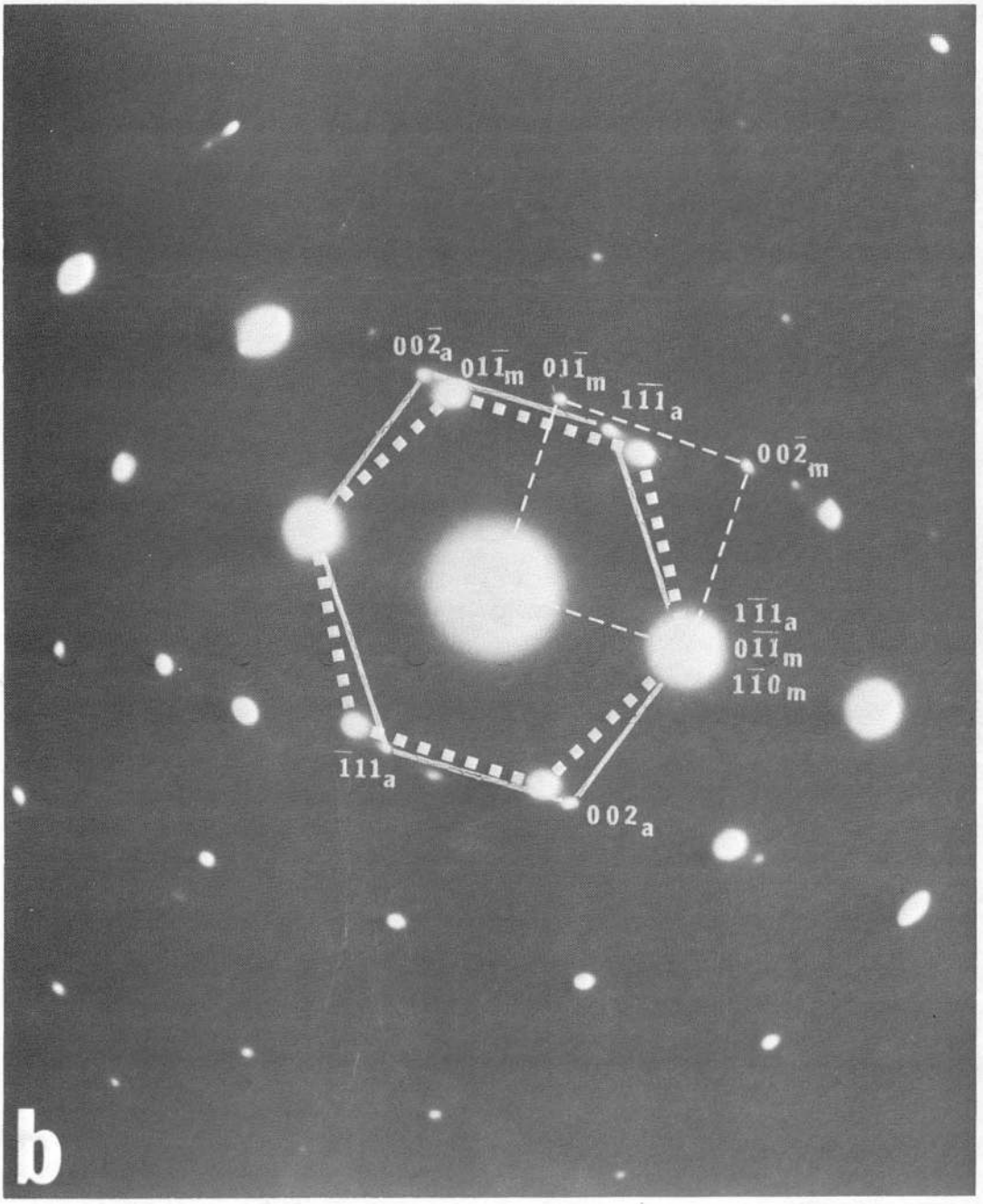

XBB 774-3113

Fig. 1(b)

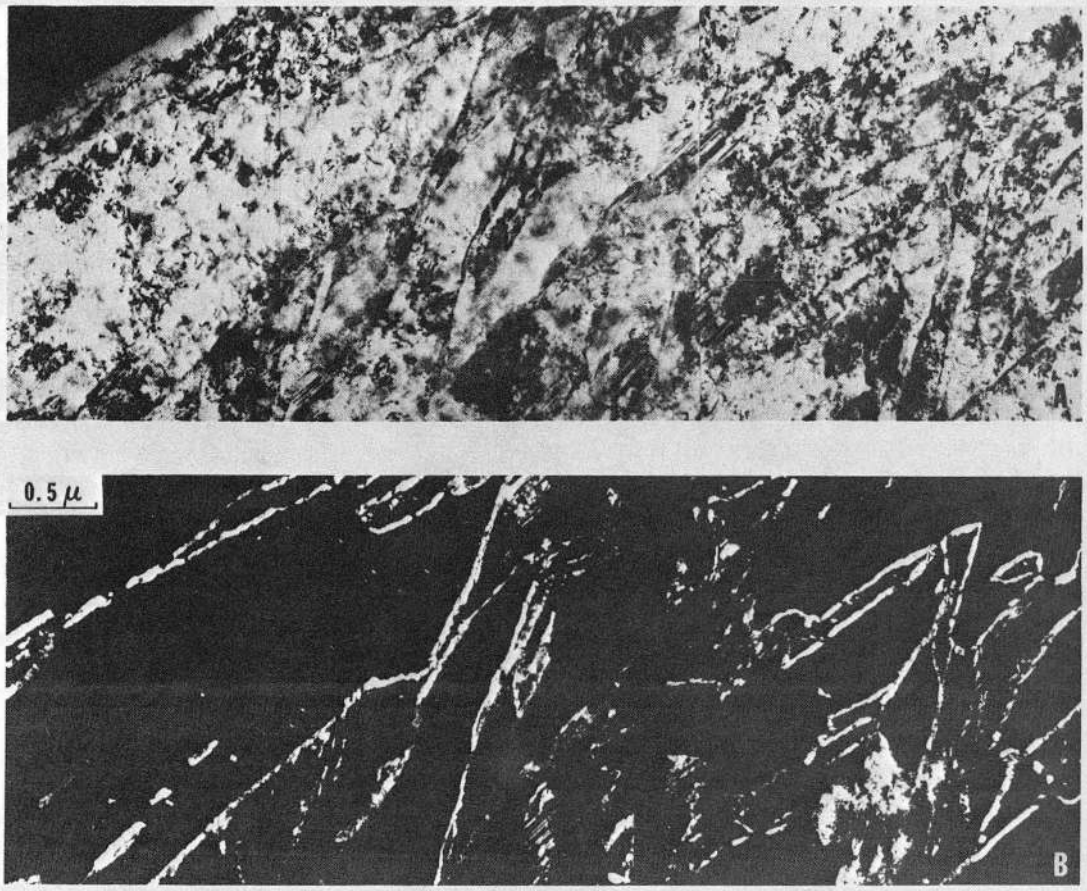

XBB 758-5825

Fig. 2

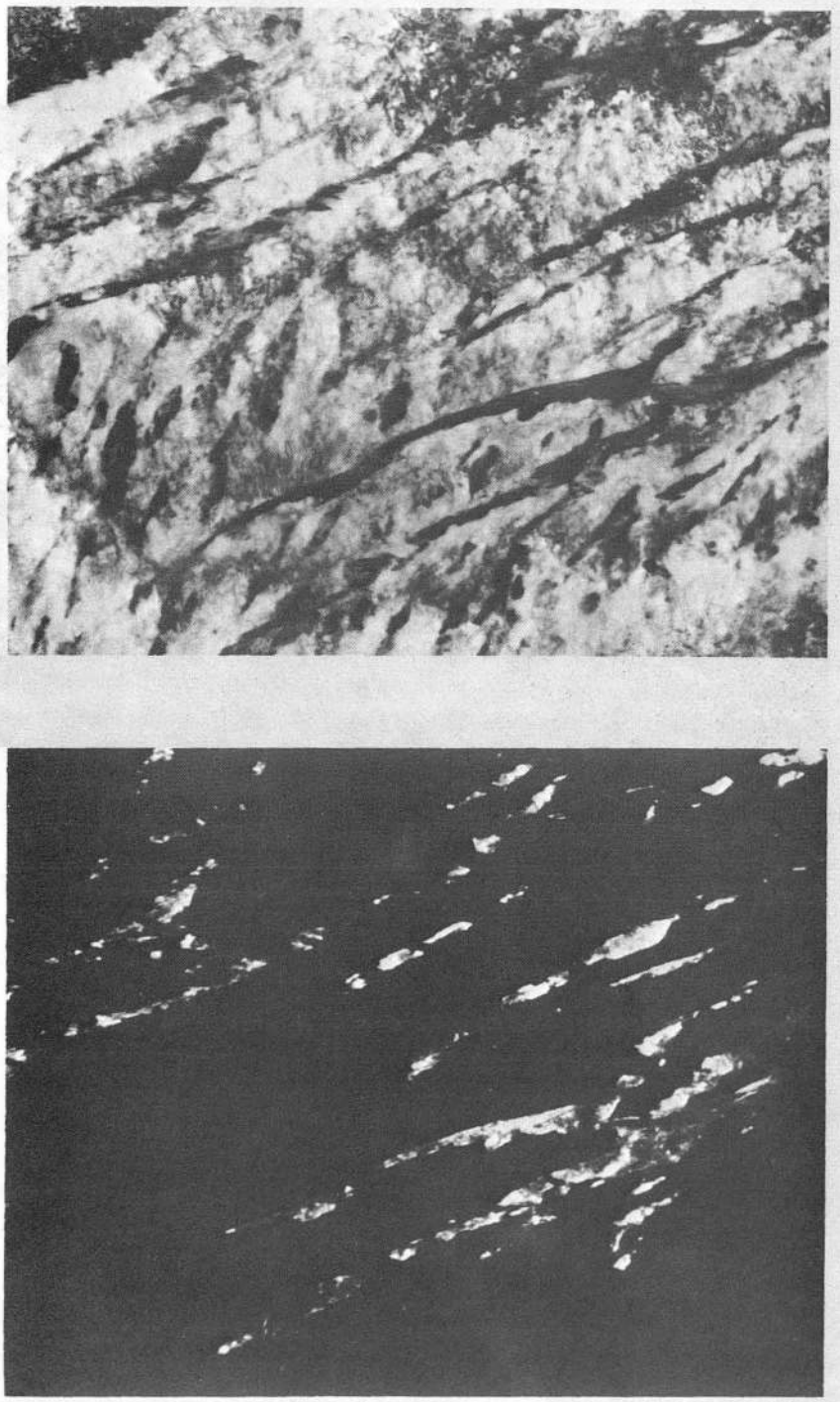

XBB 747-4387

Fig. 3

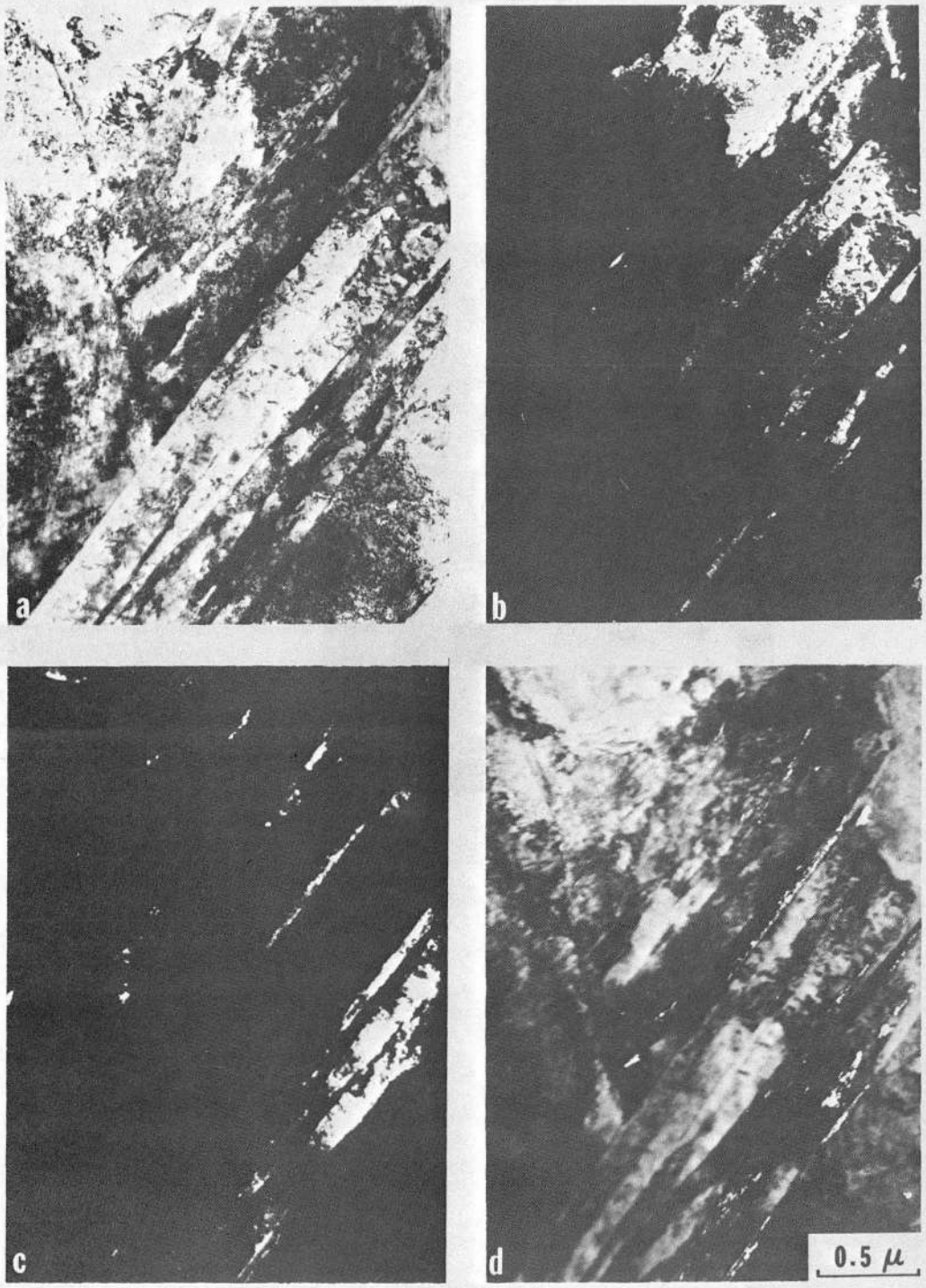

XBB 764-3836

Fig. 4(a-d)

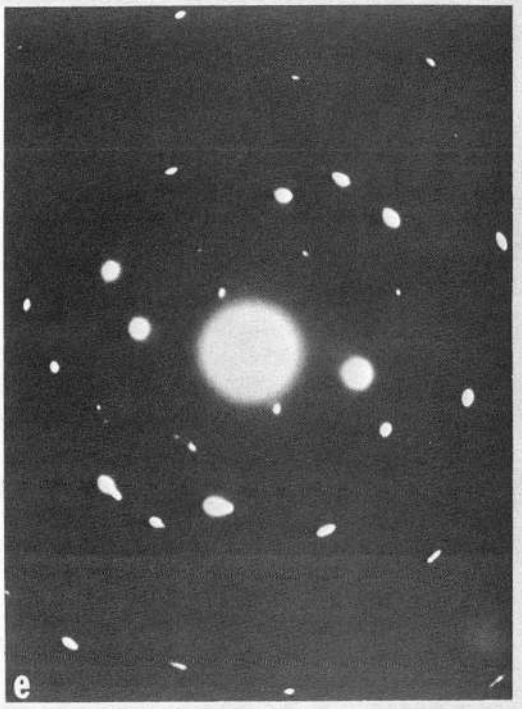

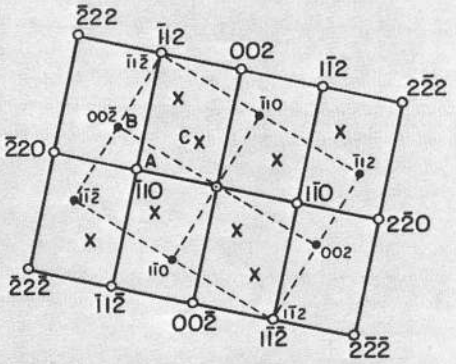

f

XBB 765-3916

Fig. 4(e-f)

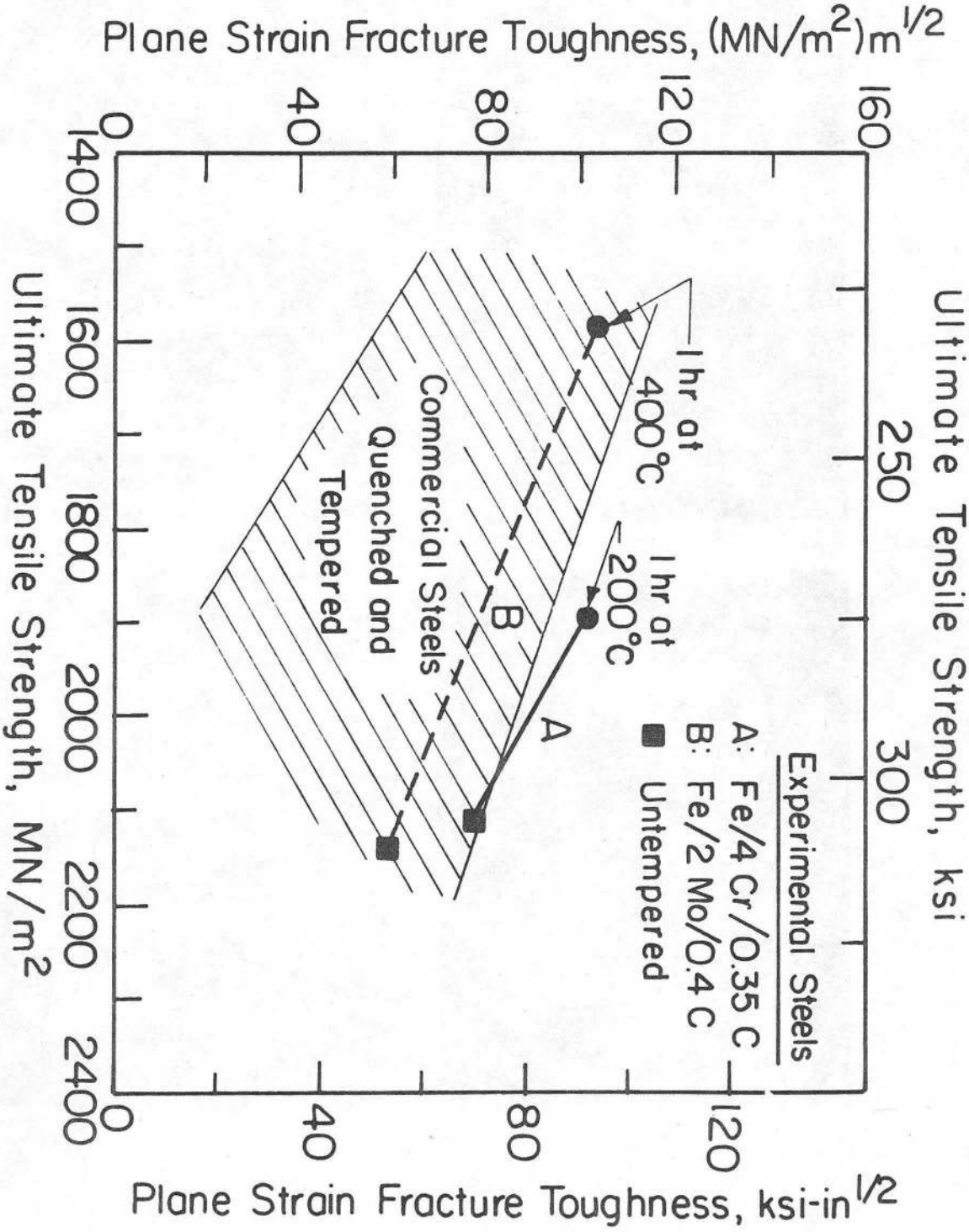

Fig. 5

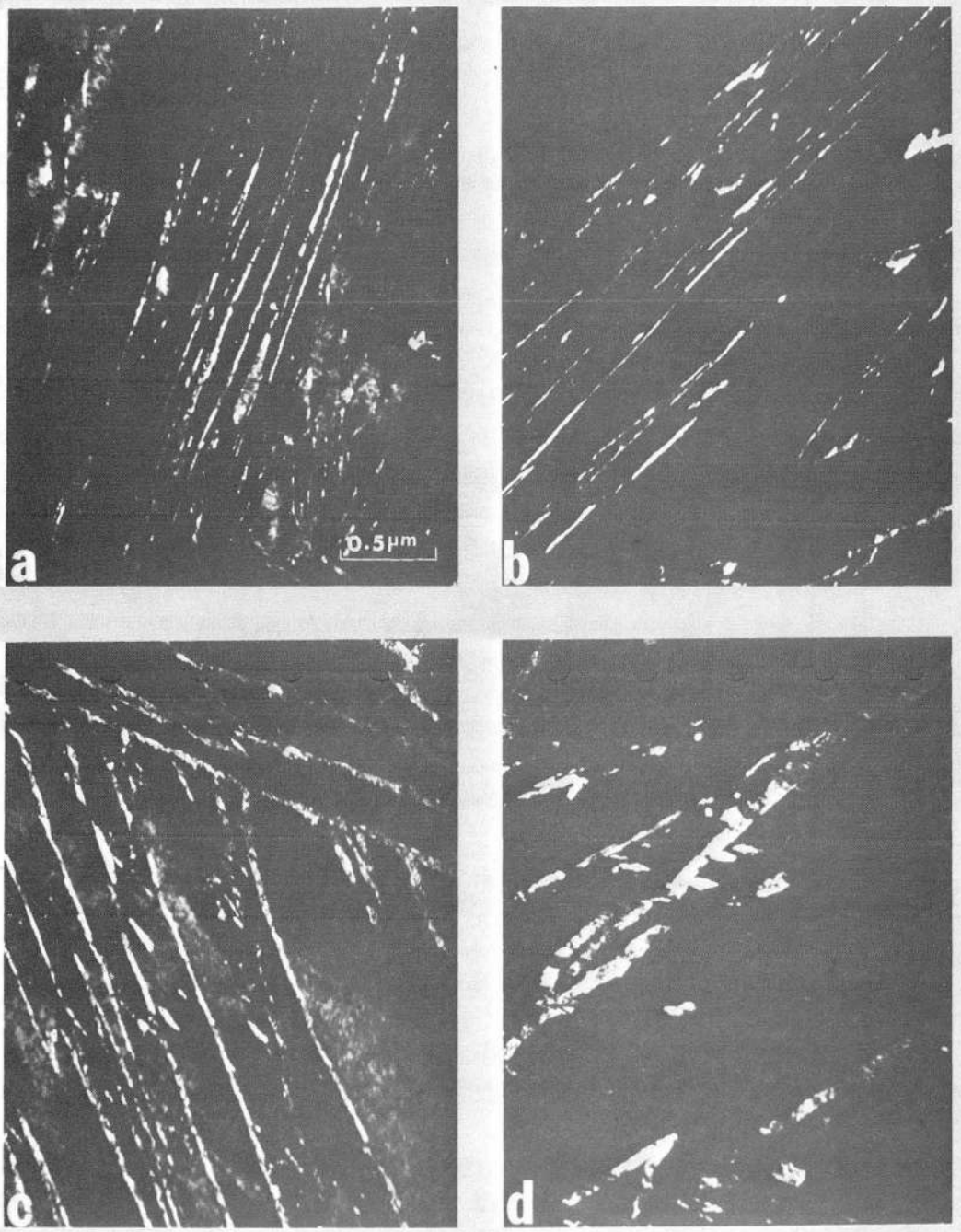

XBB 774-3111

Fig. 6(a-d)

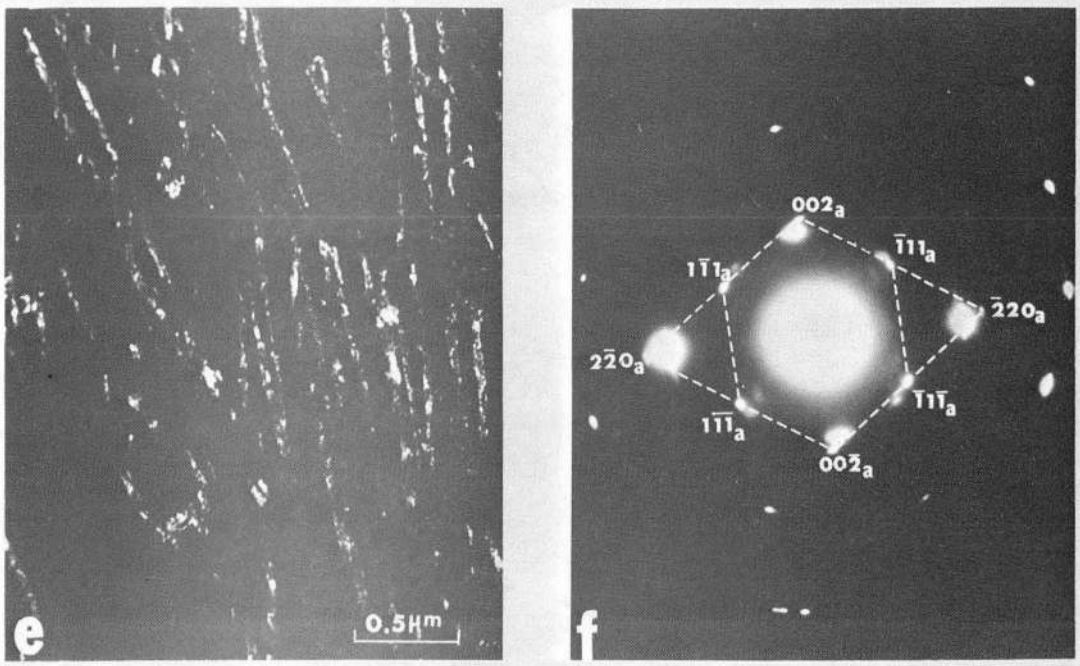

XBB 774-3112

Fig. 6(e-f)

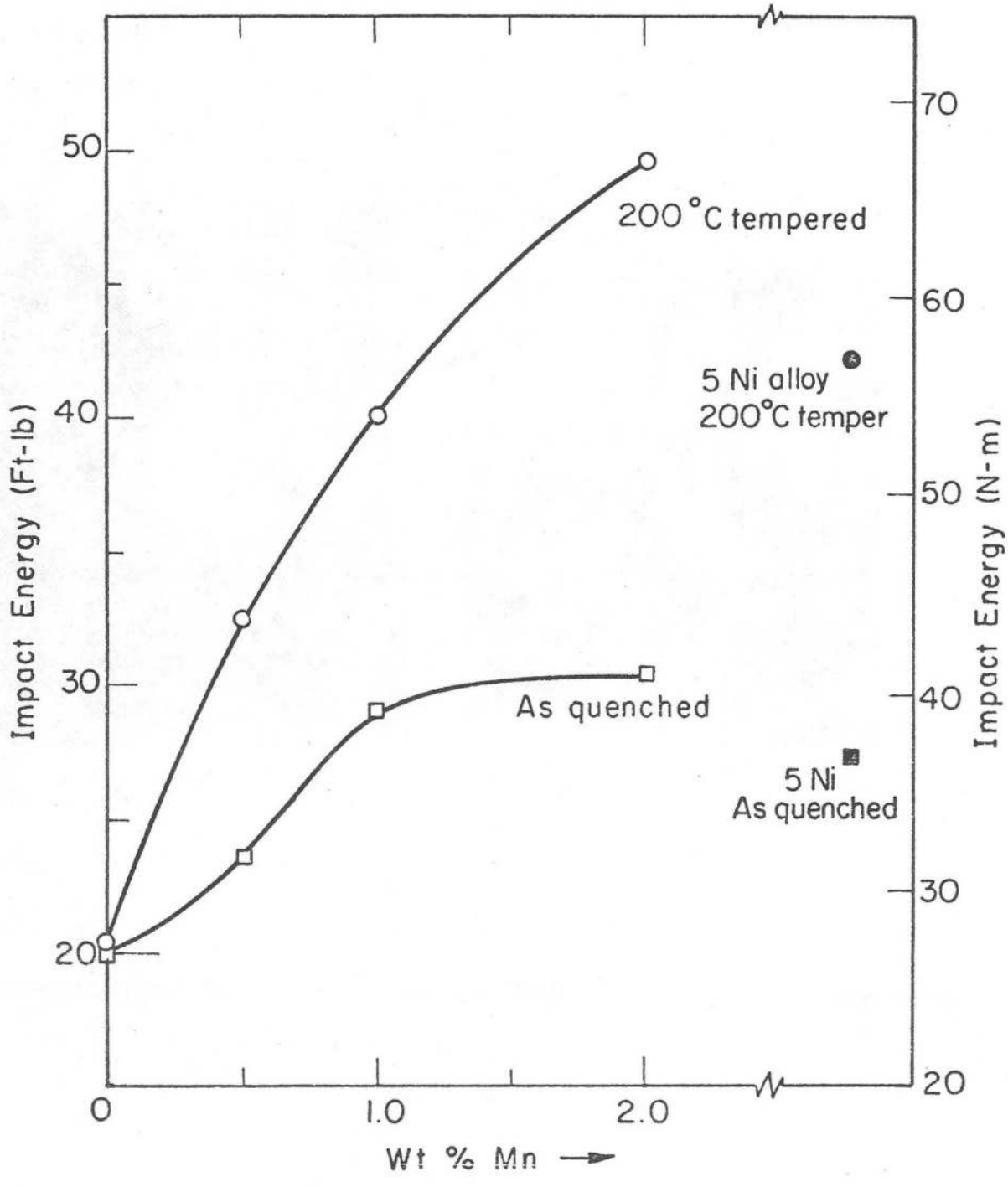
Impact Energy (Ft-lb)
Impact Energy (N-m)
50
40
30
20
70
60
50
40
30
20
200 °C tempered
5 Ni alloy
200°C temper
As quenched
5 Ni
As quenched
0
1.0
2.0
Wt % Mn
XBL 774-5303

Fig. 7

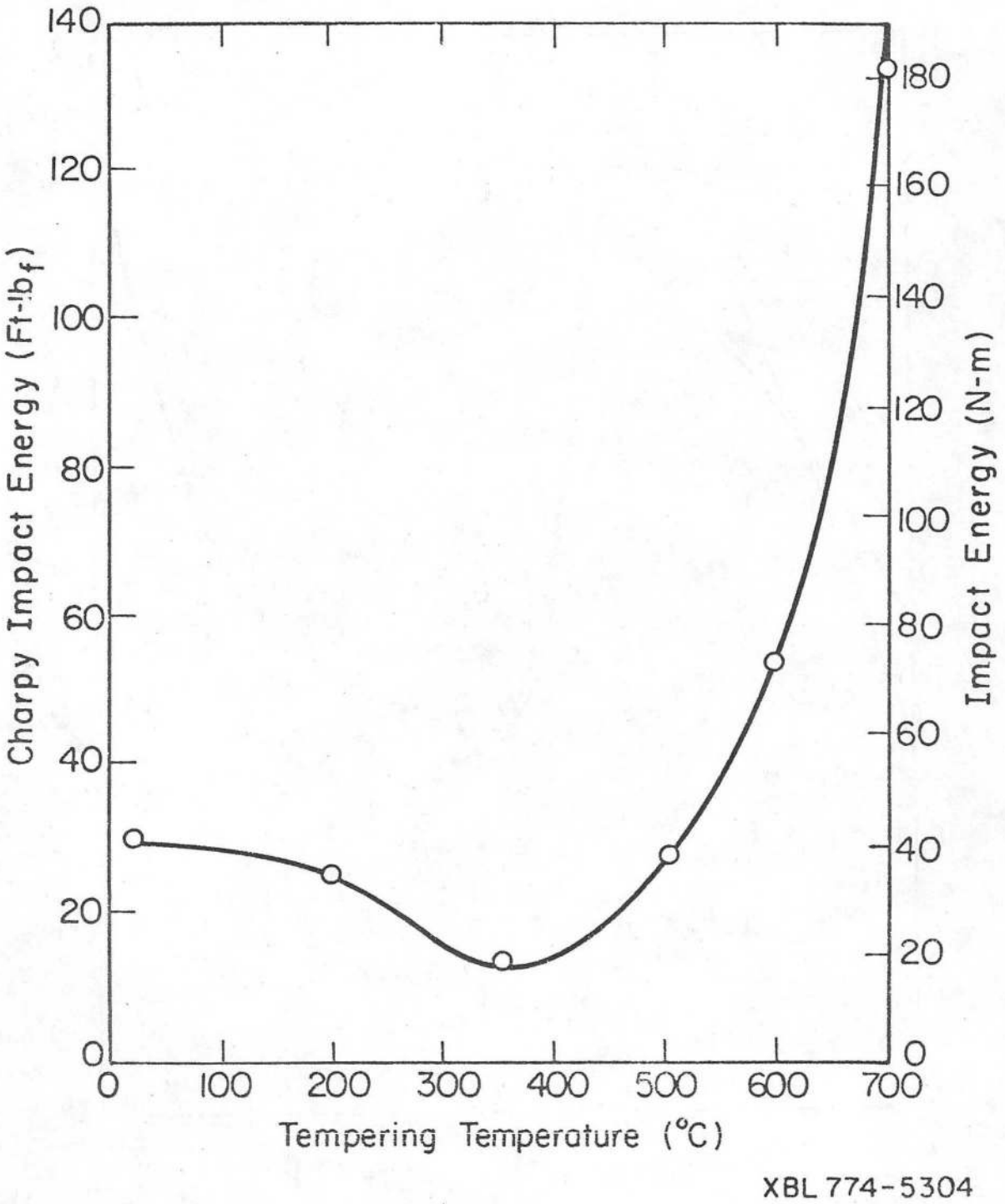
Charpy Impact Energy (Ft-lb$_f$)
Impact Energy (N-m)
Tempering Temperature (°C)
0
20
40
60
80
100
120
140
160
180
0
100
200
300
400
500
600
700
XBL 774-5304

Fig. 8(a)

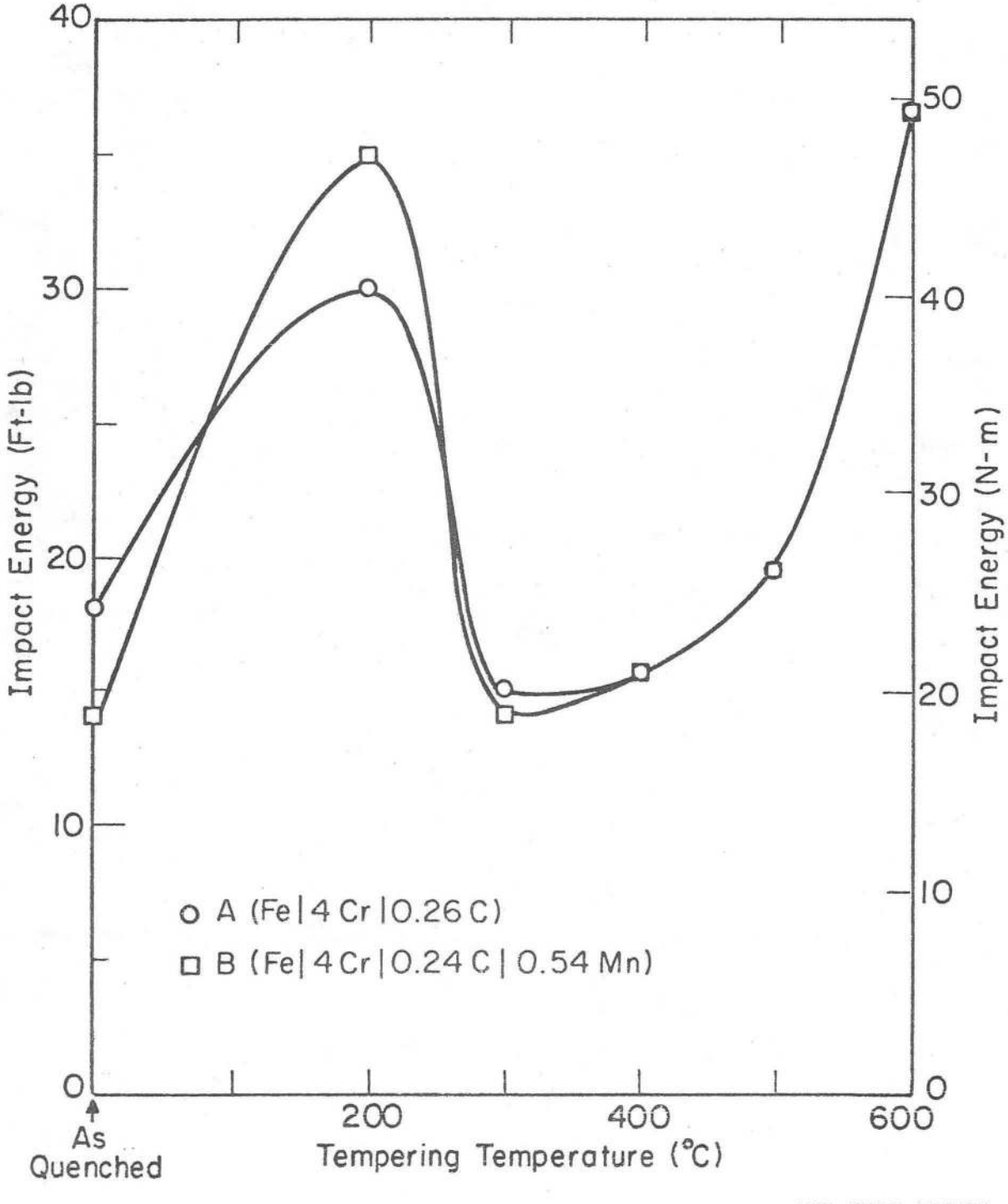
40
30
20
10
0
50
40
30
20
10
0
Impact Energy (Ft-lb)
Impact Energy (N-m)
○ A (Fe | 4 Cr | 0.26 C)
□ B (Fe | 4 Cr | 0.24 C | 0.54 Mn)
As Quenched
200
400
600
Tempering Temperature (°C)
XBL 774-5302

Fig. 8(b)

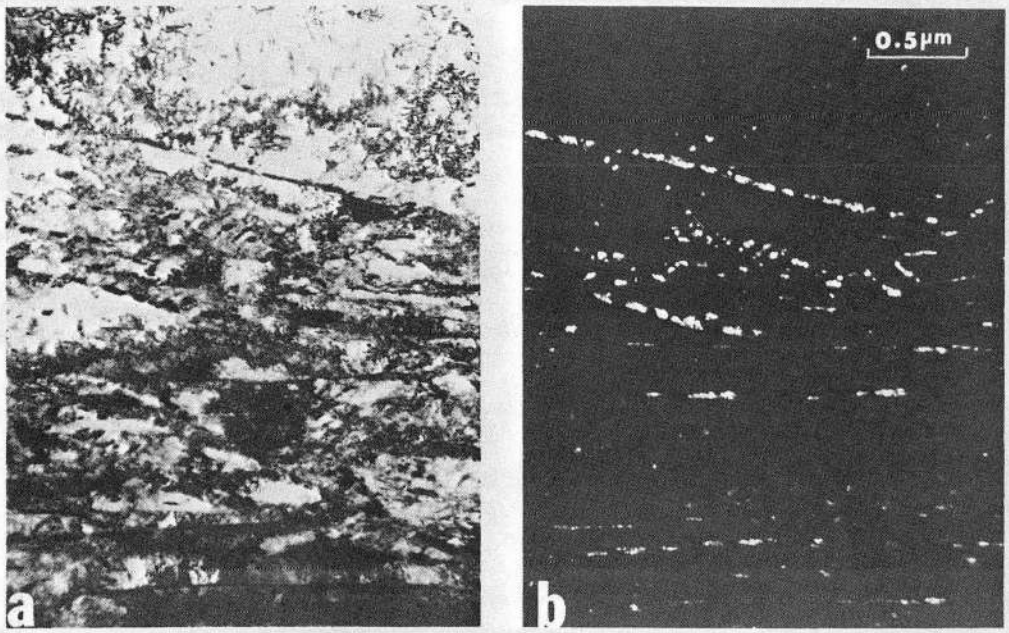

XBB 774-3114

Fig. 9(a,b)

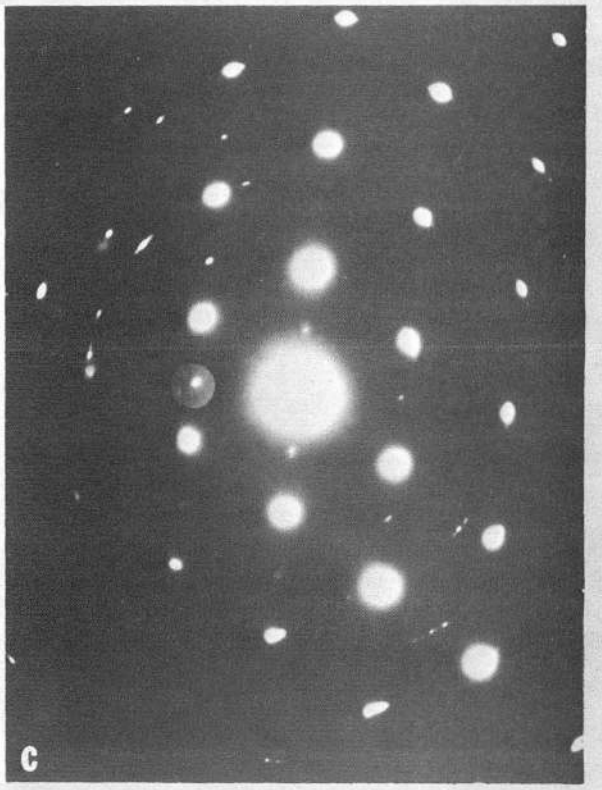

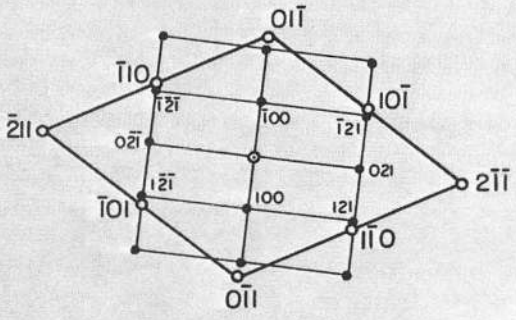

XBB 765-3913

Fig. 9(c,d)

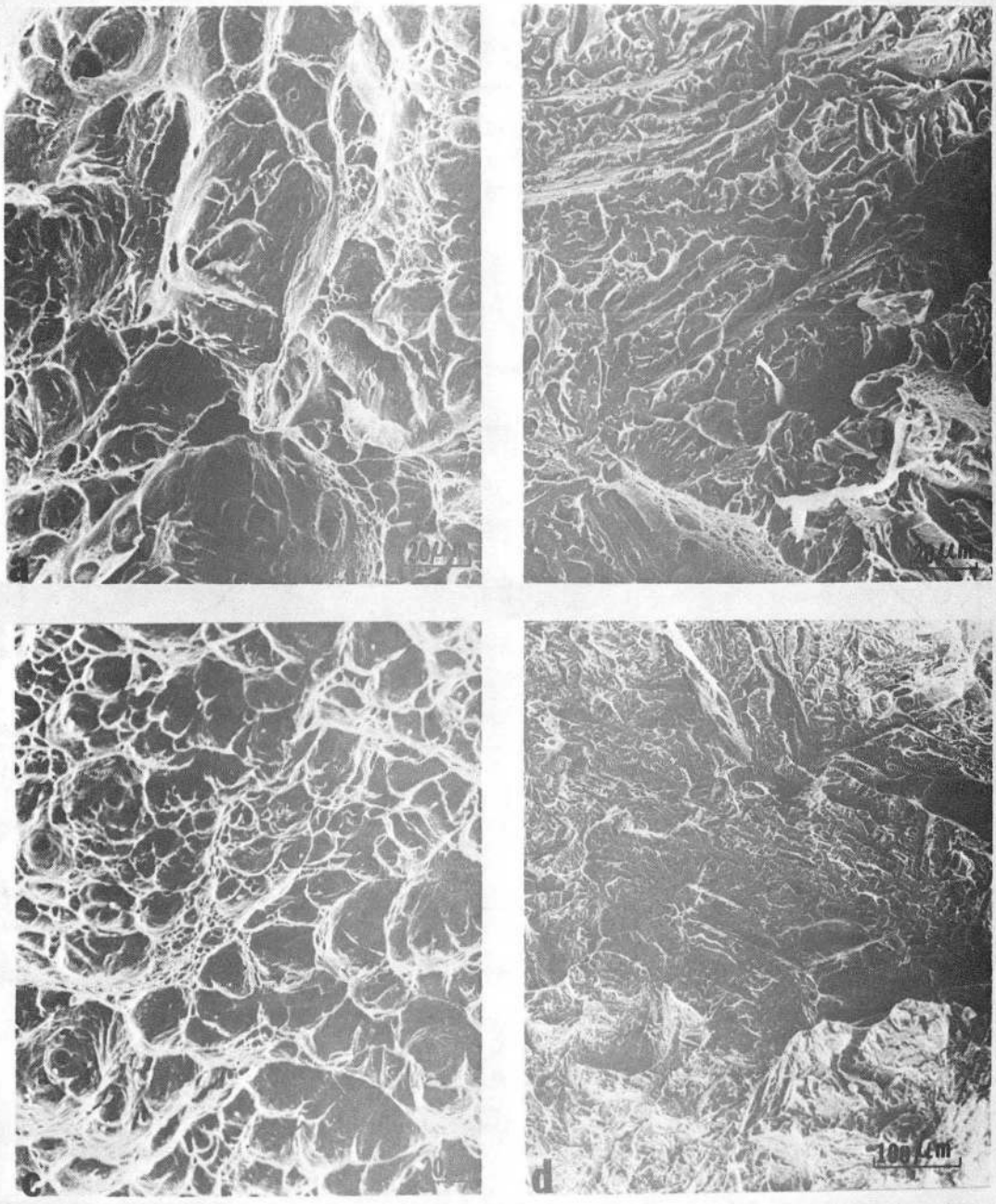

XBB 774-3110

Fig. 10

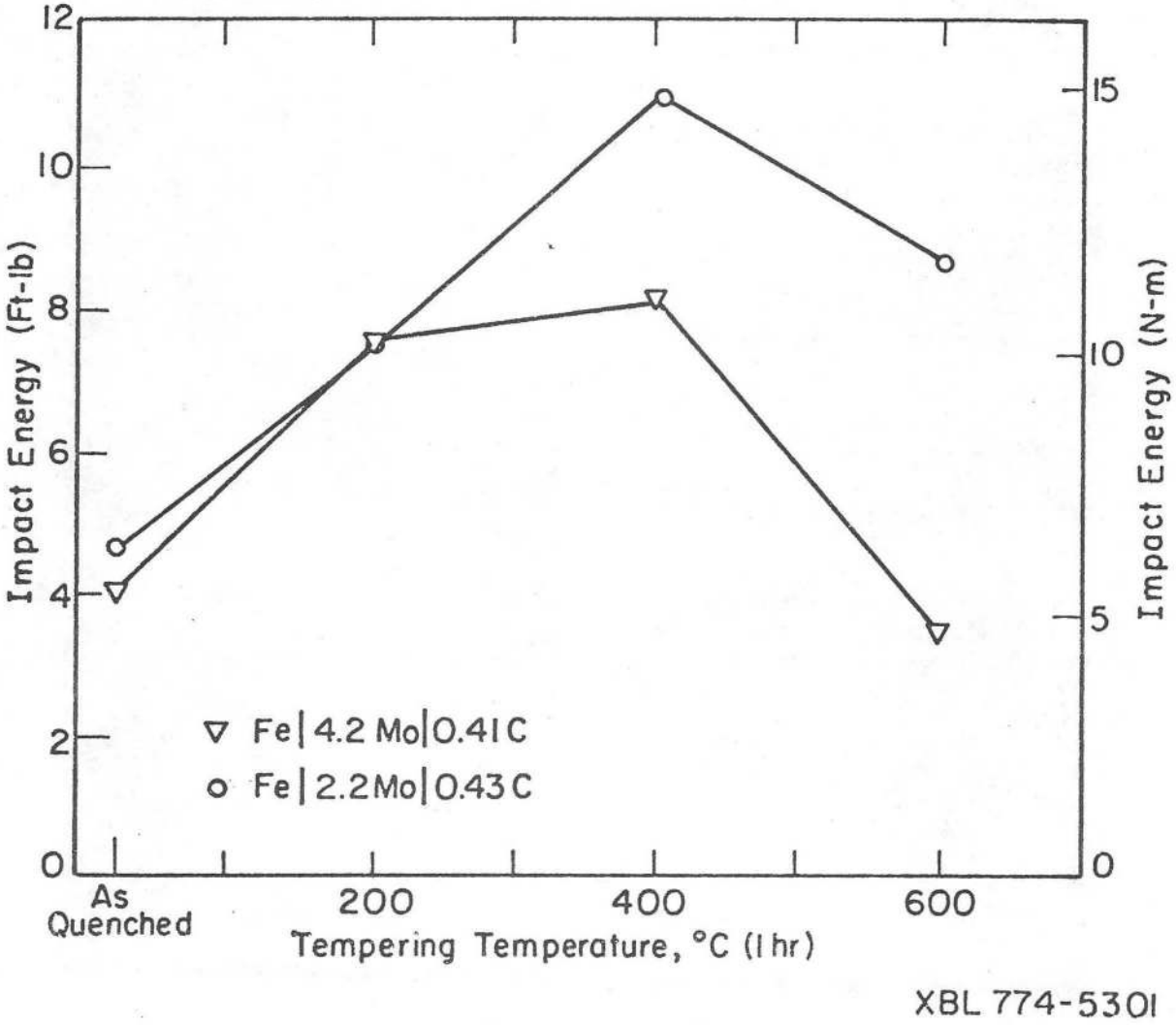
12
10
8
6
4
2
0
Impact Energy (Ft-lb)
15
10
5
0
Impact Energy (N-m)
▽ Fe | 4.2 Mo | 0.41 C
○ Fe | 2.2 Mo | 0.43 C
As Quenched
200
400
600
Tempering Temperature, °C (1 hr)
XBL 774-5301

Fig. 11

TECHNICAL INFORMATION DEPARTMENT
LAWRENCE BERKELEY LABORATORY
UNIVERSITY OF CALIFORNIA
BERKELEY, CALIFORNIA 94720